ACS OMEGA

Open Access

http://pubs.acs.org/journal/acsodf

Article

Acyclic Triterpenoids from *Alpinia katsumadai* Seeds with Proprotein Convertase Subtilisin/Kexin Type 9 Expression and Secretion Inhibitory Activity

Chae-Yeong An, Min-Gyung Son, and Young-Won Chin*

Cite This: *ACS Omega* 2023, 8, 32804−32816

Read Online

ACCESS | Metrics & More | Article Recommendations | Supporting Information

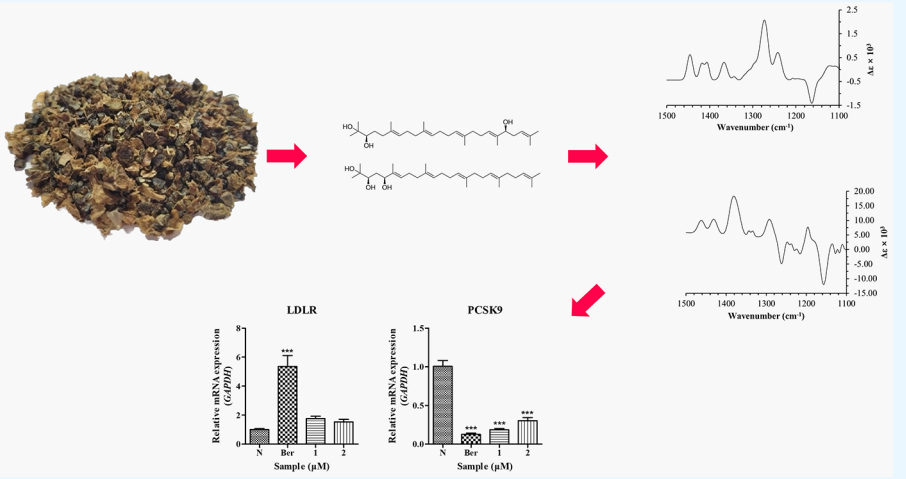

ABSTRACT: Cholesterol is one of the primary causes of cardiovascular disease. Investigating and developing potential drugs to effectively treat hypercholesterolemia are therefore of critical importance. Proprotein convertase subtilisin/kexin type 9 (PCSK9) inhibitors have been developed to lower the levels of low-density lipoprotein cholesterol in patients with hypercholesterolemia. In this study, we aimed to identify compounds that inhibit the PCSK9 mRNA expression and secretion. The bioassay-guided investigation of *Alpinia katsumadai* seeds utilizing a PCSK9 mRNA expression monitoring assay yielded the isolation and identification of seven new compounds. Among these were three acyclic triterpenoids (**1**−**3**), an acyclic sesquiterpenoid (**5**), one arylpentanoid (**6**), and two diarylheptanoids (**7** and **8**), alongside 10 known compounds. The structures of these compounds were determined using nuclear magnetic resonance (NMR) spectroscopy, vibrational circular dichroism (VCD), and electronic circular dichroism (ECD). The absolute configurations of compounds **1** and **2** were identified by comparing the calculated and experimental VCD data as the ECD method was unable to distinguish the diastereomers. All the isolated compounds were evaluated for their regulatory effects on the low-density lipoprotein receptor (LDLR) and PCSK9 mRNA expression, as well as PCSK9 secretion. Of the tested compounds, two of the acyclic triterpenoids (**1** and **2**) demonstrated potent effects in downregulating PCSK9 at both the mRNA and protein levels, compared with the positive control (berberine chloride). Additionally, compound **1** inhibited PCSK9 secretion to a level comparable to that of berberine chloride. This study identifies compounds that inhibit PCSK9 mRNA expression and secretion, offering significant contributions to the development of novel drugs for the effective treatment of hypercholesterolemia..

INTRODUCTION

Cholesterol plays a crucial role in the composition of cell membranes and serves as a precursor for the synthesis of steroid hormones as well as a cofactor for nerve signaling substances. The majority of cholesterol in the human body is produced in the liver and transported to other organs in the form of low-density lipoprotein cholesterol (LDL-C).[1,2] Elevated levels of LDL-C in the bloodstream, known as hypercholesterolemia, can lead to the development of atherosclerotic plaque, thereby increasing the risk of cardiovascular disease (CVD).[3] Considering that cholesterol

Received: June 1, 2023
Accepted: August 1, 2023
Published: August 25, 2023

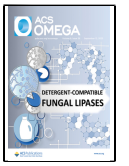

is the primary risk factor for CVD, there is an ongoing interest in the discovery of drugs that effectively treat hypercholesterolemia.[4]

Proprotein convertase subtilisin/kexin type 9 (PCSK9) plays a crucial role in the regulation of LDL-C levels in the bloodstream.[4] It functions by binding to the LDL receptor (LDLR) found in hepatic cells, thereby facilitating the internalization and degradation of the receptor. As a result, the ability of the liver to remove LDL-C from the blood is diminished.[5] Recently, PCSK9 inhibitors were developed to reduce LDL-C levels in patients with hypercholesterolemia. Among these inhibitors are two antibody drugs (alirocumab and evolocumab) and one siRNA drug (inclisiran), which have been approved for clinical use. However, a small-molecule-derived PCSK9 inhibitor of natural or synthetic origin is yet to be developed.[6−8]

Alpinia katsumadai Hayata belongs to the Zingiberaceae family and is mainly cultivated in Southeast Asia and southern China. The dried seeds of *A. katsumadai*, known as Cho Dou Kou in Korean, are commonly used as a spice in food and have a history of traditional medicinal use for treating various gastric disorders like diarrhea, abdominal pain, and emesis.[9,10] Extracts from dried *A. katsumadai* seeds exhibit a range of pharmacological properties, including antioxidative, antiviral, and anticancer, and the induction of heat shock proteins.[11] They have also demonstrated hypolipidemic effects.[11] Due to its traditional use for digestive issues, there has been interest in exploring its potential to lower cholesterol levels in the bloodstream. Previous studies have shown that 50% ethanolic extracts of *A. katsumadai* displayed significant inhibitory activity in fatty acid synthase inhibition assays, while the chloroform fraction of these extracts reduced plasma levels in high cholesterol-fed rats.[11,12] Phytochemical investigations have identified various constituents in *A. katsumadai* extracts including diarylheptanoids, kavalactones, flavonoids, stilbenes, monoterpenes, sesquiterpenes, and triterpenes. Among these compounds, chalcones were found to prevent lipid accumulation, and acyclic triterpenoids were found to inhibit cholesterol acyl transferase activity.[13,14] As part of our ongoing study,[15,16] we conducted bioassay-guided isolation to identify compounds that have PCSK9 mRNA expression inhibitory activities. Based on *in vitro* experiments, it was found that the hexane-soluble fraction exhibited the highest activity. This fraction notably decreases PCSK9 mRNA expression while not downregulating LDLR mRNA expression (Figure S84). Subsequently, the active fractions of the hexane-soluble fraction, which demonstrated an inhibitory activity against PCSK9 mRNA, were selected for further isolation.

Various chromatographic methods were employed to isolate 17 compounds from the *n*-hexane fraction of the methanol extract obtained from *A. katsumadai* seeds. Among these compounds, seven were new (**1**−**3** and **5**−**8**), and the remaining 10 were known compounds (**4** and **9**−**17**). The structures of these compounds were elucidated by using a combination of physicochemical and spectroscopic techniques. Subsequently, all of the isolated compounds were assessed for their inhibitory effects on PCSK9 expression and secretion.

RESULTS AND DISCUSSION

Compound **1**, obtained as colorless oil, displayed a sodium adduct ion peak at *m*/*z* 483.3814 $[M + Na]^+$ (calcd for $[C_{30}H_{52}O_3Na]^+$, 483.3814) with five degrees of unsaturation in high-resolution electrospray ionization mass spectrometry

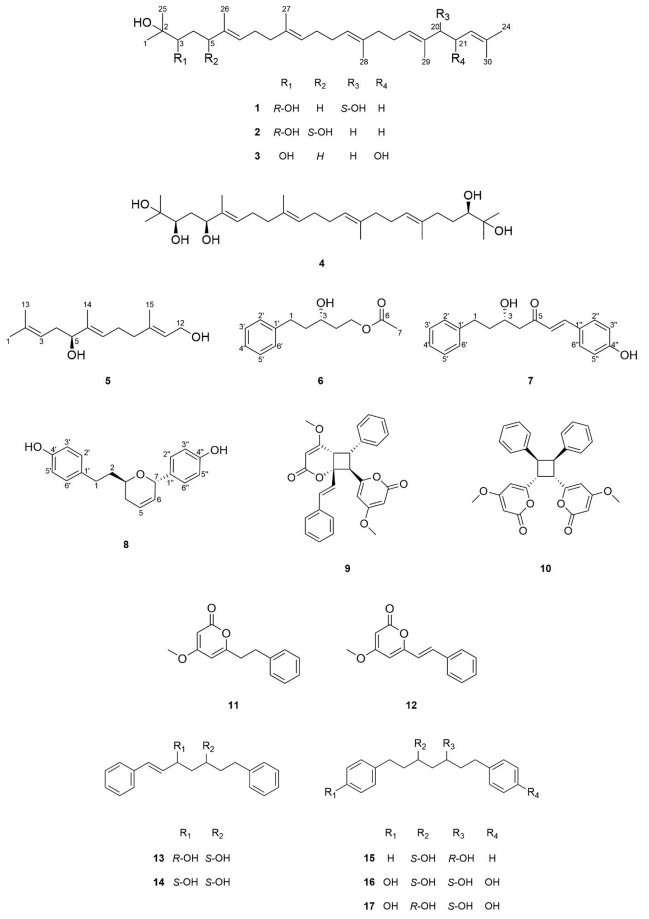

(HRESIMS). In the ultraviolet (UV) spectrum, compound **1** exhibited an absorption band at 202 nm, while the infrared (IR) spectrum indicated absorption bands at 3393 cm^{-1} for hydroxy groups and 2923 cm^{-1} for methyl groups. Proton nuclear magnetic resonance (^{1}H NMR) spectroscopic data of compound **1** exhibited signals corresponding to five olefinic groups at δ_H 5.19 (1H, br t, J = 6.2 Hz, H-7), 5.15 (2H, overlapped, H-11, H-14), 5.39 (1H, br t, J = 6.9 Hz, H-18), and 5.09 (1H, br t, J = 7.1 Hz, H-22), two oxygenated methines at δ_H 3.34 (1H, br d, J = 10.5, Hz, H-3) and 3.98 (1H, dd, J = 7.8, 5.5 Hz, H-20), methylenes at δ_H 1.42−2.28 (H-4, H-5, H-8, H-9, H-12, H-13, H-16, H-17, H-21), four methyls at δ_H 1.16 (3H, s, H-1), 1.72 (3H, s, H-24), 1.20 (3H, s, H-25), and 1.64 (3H, s, H-30), and remaining methyl groups at δ_H 1.60−1.62 (H-26, H-27, H-28, H-29). Carbon nuclear magnetic resonance (^{13}C NMR), distortion enhancement by polarization transfer (DEPT), and heteronuclear single−quantum correlation (HSQC) spectroscopic data of compound **1** displayed the presence of 30 carbon signals. This consisted of six quaternary carbons [including five olefinic carbons at δ_C 135.0 (C-6), 134.9 (C-10, C-15), 136.7 (C-19), and 134.7 (C-23) and one oxygenated carbon at δ_C 73.0 (C-2)], five olefinic carbons at δ_C 125.1 (C-7), 124.5 (C-11, C-14) 126.2 (C-18), and 120.3 (C-22), two oxygenated methine carbons at δ_C 78.3 (C-3) and 77.3 (C-20), nine methylene carbons at δ_C 29.6 (C-4), 36.9 (C-5), 26.5 (C-8), 39.7 (C-9), 28.2 (C-12, C-13), 39.4 (C-16), 26.2 (C-17), and 34.2 (C-21) and eight methyls at δ_C 23.3 (C-1), 25.9 (C-24), 26.4 (C-25), 15.9 (C-26), 16.0 (C-27, C-28), 11.7 (C-29), and 18.0 (C-30) (Table 1). These ^{1}H and ^{13}C NMR spectroscopic data suggest

https://doi.org/10.1021/acsomega.3c03873
ACS Omega 2023, 8, 32804−32816

Table 1. ^{1}H and ^{13}C NMR Spectroscopic Data of Compounds 1−3 in $CDCl_3$

position	1[a]		2[b]		3[b]	
	δ_C, type	δ_H (J in Hz)	δ_C, type	δ_H (J in Hz)	δ_C	δ_H (J in Hz)
1	23.3 CH_3	1.16, s	23.8 CH_3	1.17, s	23.3 CH_3	1.15, s
2	73.0C		72.5C		73.0C	
3	78.3 CH	3.34, br d (10.5)	78.7 CH	3.62, dd (8.7, 3.5)	78.3 CH	3.35, br d (10.5)
4	29.6 CH_2	1.42, m	35.9 CH_2	1.64, overlapped	29.6 CH_2	1.41, m
		1.59, overlapped				1.57, overlapped
5	36.9 CH_2	2.11, overlapped	78.6 CH	4.27, dd (8.5, 4.3)	36.8 CH_2	2.09, overlapped
		2.21, overlapped				2.21, overlapped
6	135.0C		137.1C		134.8C	
7	125.1 CH	5.19, br t (6.2)	126.5 CH	5.43, br t (6.9)	125.1 CH	5.23, br t (7.0)
8	26.5 CH_2	2.11, overlapped	26.1 CH_2	2.12, m	26.5 CH_2	2.11, overlapped
9	39.7 CH_2	2.02, overlapped	39.3 CH_2	2.01, overlapped	39.7 CH_2	2.01, overlapped
		2.11, overlapped				
10	134.9C		134.7C		135.0C	
11	124.5 CH	5.15, overlapped	124.4 CH	5.12, overlapped	124.5 CH	5.15, overlapped
12	28.2 CH_2	2.02, overlapped	28.3 CH_2	2.01, overlapped	28.2 CH_2	2.01, overlapped
13	28.2 CH_2	2.02, overlapped	26.8 CH_2	2.07, overlapped	28.2 CH_2	2.01, overlapped
14	124.5 CH	5.15, overlapped	124.2 CH	5.12, overlapped	124.7 CH	5.15, overlapped
15	134.9C		135.3C		134.9C	
16	39.4 CH_2	2.02, overlapped	39.7 CH_2	1.98, overlapped	39.6 CH_2	2.01, overlapped
17	26.2 CH_2	2.11, overlapped	28.3 CH_2	2.01, overlapped	26.5 CH_2	2.11, overlapped
18	126.2 CH	5.39, br t (6.9)	124.2 CH	5.12, overlapped	128.7 CH	5.19, br t (7.1)
19	136.7C		135.0C		131.6C	
20	77.3 CH	3.98, dd (7.8, 5.5)	39.7 CH_2	1.98, overlapped	48.2 CH_2	2.11, overlapped
21	34.2 CH_2	2.21, overlapped	26.7 CH_2	2.07, overlapped	65.6 CH	4.40, td (8.4, 4.6)
		2.28, m				
22	120.3 CH	5.09, br t (7.1)	124.7 CH	5.12, overlapped	127.4 CH	5.15, overlapped
23	134.7C		131.3C		134.8C	
24	25.9 CH_3	1.72, s	17.7 CH_3	1.60, overlapped	25.8 CH_3	1.72, s
25	26.4 CH_3	1.20, s	26.3 CH_3	1.21, s	26.4 CH_3	1.20, s
26	15.9 CH_3	1.62, overlapped	11.6 CH_3	1.68, overlapped	16.0 CH_3	1.62, s
27	16.0 CH_3	1.60, s	16.0 CH_3	1.60, overlapped	15.9 CH_3	1.60, overlapped
28	16.0 CH_3	1.61, s	16.0 CH_3	1.60, overlapped	15.9 CH_3	1.60, overlapped
29	11.7 CH_3	1.62, overlapped	16.1 CH_3	1.60, overlapped	16.1 CH_3	1.66, s
30	18.0 CH_3	1.64, s	25.7 CH_3	1.68, s	18.2 CH_3	1.69, s

[a]Recorded at ^{1}H (400 MHz) and ^{13}C (100 MHz). [b]Recorded at ^{1}H (500 MHz) and ^{13}C (125 MHz).

that compound **1** belongs to the class of acyclic triterpenoids identified in this plant.[14,17−19] The $^{1}H-^{1}H$ correlation spectroscopy (COSY) cross-peaks indicated the presence of six spin−spin coupling systems of H-3/H_2-4/H_2-5, H-7/H_2-8, H-11/H_2-12, H_2-13/H-14, H_2-17/H-18, and H-20/H_2-21/H-22 (Figure 1). Along with $^{1}H-^{1}H$ COSY data, the heteronuclear multiple bond correlations (HMBC) from Me-1/Me-25 to C-2/C-3, H_2-5/Me-26 to C-6/C-7, H_2-9/Me-27 to C-10/C-11, H_2-16/Me-28 to C-14/C-15, H-20/Me-29 to C-18/C-19, and Me-24/Me-30 to C-22/C-23 enabled the construction of six isoprene moieties. Moreover, the HMBC from H-3 to C-5 and H-7 to C-9 were assigned to the structure of **1a** and the HMBC from H_2-16 to C-18 and H-20 to C-22 were assigned to the structure of **1b**. The linkage between **1a** and **1b** was confirmed by HMBC from H-11 to C-13. Based on these data, the planar structure of compound **1** was established as an acyclic triterpenoid belonging to the class of 2,3-oxidosqualene, which could be the precursor for cyclic triterpenoids (Figure 1).[20,21] Although several acyclic triterpenoids have been reported in the same species, the structure of compound **1** has not been described previously.[14,17−19]

The spectroscopic data were not sufficient to analyze the relative configuration of compound **1** due to the complexity and overlap of the NMR data as well as the simplicity of its UV spectrum. The conformational flexibility of compound **1** resulted in a large number of conformers. However, the electronic circular dichroism (ECD) spectra were calculated, and the results were compared to the experimental ECD spectra of compound **1** (Figures S69 and S71). The calculated ECD spectra of diastereomers (3*R*,20*S*)-**1** or (3*S*,20*S*)-**1** generated by the computational calculations were in good agreement with the experimental ECD spectra for compound **1** at the mPW1PW91/6-31+G (d, p) calculation (Figure S69). Furthermore, the ECD spectra calculated at the B3LYP/6-31+G (d, p) level of theory exhibited similarity to those of either (3*R*,20*R*)-**1** or (3*S*,20*R*)-**1** (Figure S71). This indicated that the ECD method was unable to differentiate between the diastereomers of this type of skeleton. As ECD is a technique based on electron distribution, it requires a chromophore that undergoes structural changes involving electron movement within the molecule. The hydroxyl group at position C-3 in compounds **1** and **2** is located in a region that is not influenced by the chromophore, resulting in an ECD-silent position. Therefore, the ECD spectrum alone was unable to distinguish

https://doi.org/10.1021/acsomega.3c03873
ACS Omega 2023, 8, 32804−32816

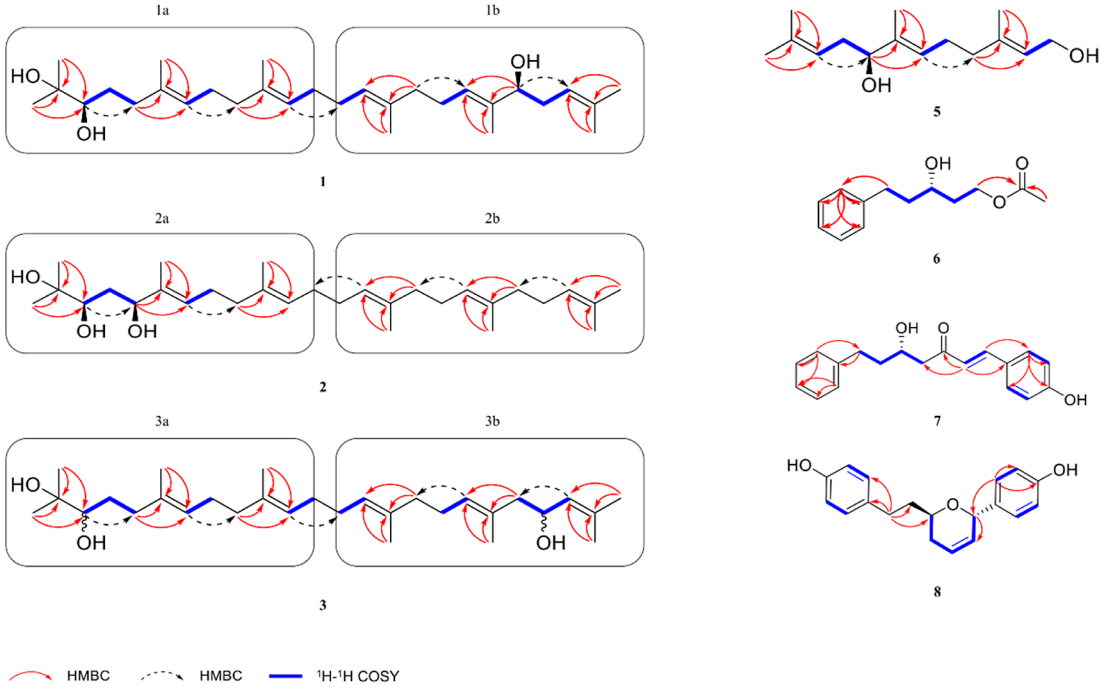

Figure 1. Key HMBC and $^{1}H-^{1}H$ COSY correlations of compounds **1**, **2**, **3**, **5**, **6**, **7**, and **8**.

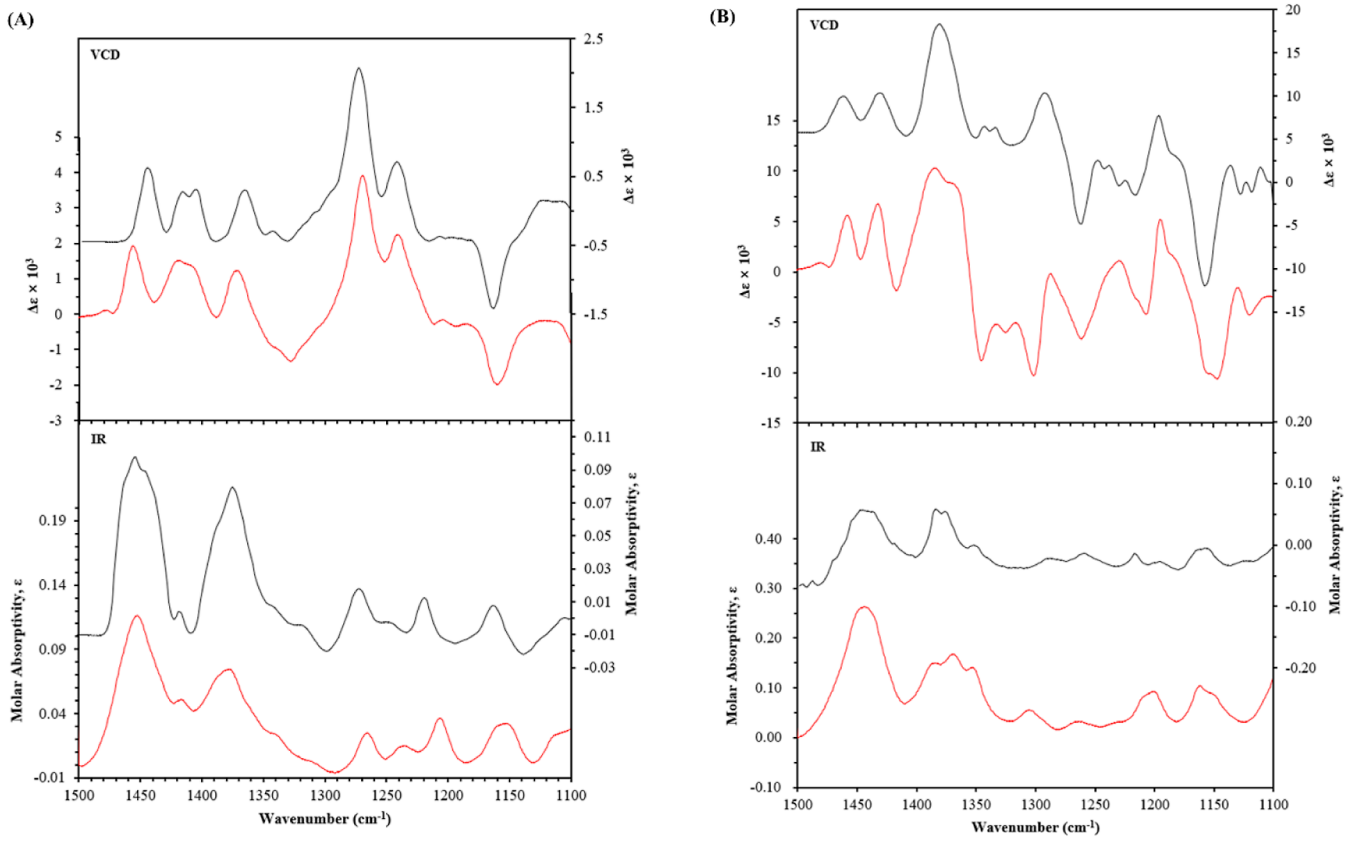

Figure 2. (A) Calculated (3*R*,20*S*-**1** (red) and experimental compound **1** (black). (B) Calculated 3*R*5*S*-**2** (red) and experimental compound **2** (black). The calculated (red) and experimental (black) VCD and IR curves employ a wavenumber correction [shift = −30 cm^{-1} (**1**) and −35 cm^{-1} (**2**), gamma value = 0.8 cm^{-1}, respectively]. All experimental spectra (black) are plotted with the *y*-axis on the right side, while calculated spectra (red) are plotted with the *y*-axis on the left side.

between the diastereomers of these compounds determining the stereochemistry of compounds **1** and **2**, and thus, it was not possible solely based on ECD. Consequently, vibrational circular dichroism (VCD) spectroscopy was employed to determine the absolute configuration. VCD spectroscopy is capable of detecting vibrational transitions of chemical bonds

https://doi.org/10.1021/acsomega.3c03873
ACS Omega 2023, 8, 32804−32816

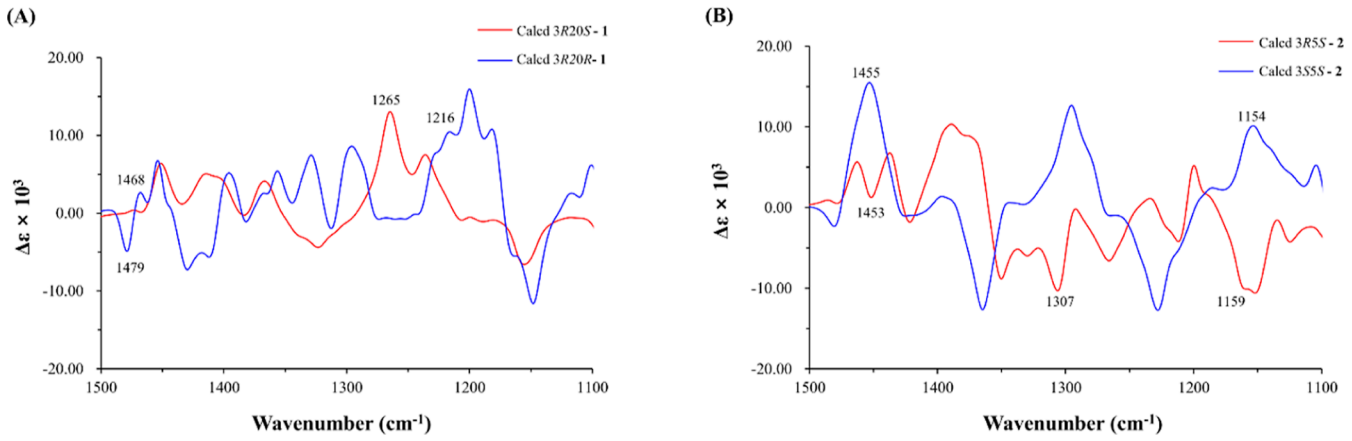

Figure 3. Calculated (red and blue) VCD curves employing a wavenumber correction [shift = −30 cm^{-1} (**1**) and −35 cm^{-1} (**2**), gamma value = 0.8 cm^{-1}, respectively].

in molecules and offers a greater number of transitions than ECD. Therefore, the VCD spectroscopic method may be more effective in detecting stereochemical or conformational changes in molecules. Furthermore, unlike ECD, VCD spectroscopy does not require chromophores for analyzing the compound of interest.[22−24] For these reasons, after experimental measurement and calculation of VCD, experimental and calculated VCD and IR spectral data of **1** were compared within the range from 1500 to 1100 wavenumbers (cm^{-1}), which is referred to as the fingerprint region (Figures 2A, S79, and S80).[25] Due to these advantages, the experimental and calculated VCD and IR spectral data of compound **1** were compared specifically in the fingerprint region ranging from 1500 to 1100 wavenumbers (cm^{-1}) (Figures 2A, S79, and S80).[25] After the comparison, the VCD and IR data demonstrated agreement with the (3*R*,20*S*)-**1** configuration, confirming that compound **1** was (3*R*,20*S*)-2,3,20-trihydroxy-2,6,10,15,19,23-hexamethyl-tetracosa-6,10,14,18,22-pentaene.

Although they share the same overall shape, the VCD spectra of the diastereomers (3*R*,20*S*)- and (3*R*,20*R*)-**1** exhibited distinct features that facilitated their differentiation (Figure 3A). The functional groups, such as C−O commonly found in alcohols, exhibit strong vibrations in the range of 1300−1000 cm^{-1}.[26] By examining the difference between the two diastereomers in Figure 3, we can observe that the opposite signs of the peaks at 1216 and 1265 cm^{-1} are associated with the stereoisomeric structure of the C−O group at position C-20. Additionally, the observation that the signs of the vibrations at 1468 and 1479 cm^{-1}, corresponding to CH_2 groups, are opposite suggests variations in the CH_2 group vibrations due to a change in the stereoisomeric structure at C-20.[26] These specific vibrational transitions at 1216, 1265, 1468, and 1479 cm^{-1} played a critical role in distinguishing between the two diastereomers. These findings underscore the advantages of utilizing VCD, instead of ECD, for determining the absolute configuration of such diastereomeric molecules.

Compound **2** was isolated as a colorless oil, and its molecular formula of $C_{30}H_{52}O_3$ was suggested from its formic acid adduct ion peak at *m*/*z* 505.3891 $[M + HCOO]^-$ (calculated for $[C_{31}H_{53}O_5]^-$, 505.3893). The ^1H NMR data for compound **2** were similar to those of compound **1**, except for the differences in the chemical shifts of five olefinic groups at δ_H 5.43 (1H, br t, *J* = 6.9 Hz, H-7) and 5.12−5.19 (4H, overlapped, H-11, H-14, H-18, H-22) and two oxygenated methines at δ_H 3.62 (1H, dd, *J* = 8.7, 3.5 Hz, H-3) and δ_H 4.27 (1H, dd, *J* = 8.5, 4.3 Hz, H-5). The HMBC between the oxygenated methine proton on C-3 and the carbon at C-5, indicated that compound **2** has a structure distinct from that of compound **1** (Table 1). The $^1H-^1H$ COSY correlation of H-3/H_2-4/H-5 and H-7/H_2-8, together with the HMBC cross-peaks from Me-1/Me-25 to C-2/C-3, H-5/Me-26 to C-6/C-7, H_2-9/Me-27 to C-10/C-11, H_2-16/Me-28 to C-14/C-15, H_2-20/Me-29 to C-18/C-19, and Me-24/Me-30 to C-22/C-23 of compound **2**, indicated the presence of six isoprene moieties. The connection of each isoprene was assigned by the HMBC between H-3 and C-5 and H-7 and C-9 for unit **2a**, H-18 and C-16 and H-22 and C-20 for unit **2b**. The link between units **2a** and **2b** was confirmed by the HMBC between H-14 and C-12, which suggests a planar structure of compound **2** (Figure 1). Similar to compound **1**, the calculated ECD spectra of compound **2** did not provide a distinction between the diastereomers (Figures S69 and S71). Consequently, VCD measurements and calculations were carried out to determine the absolute configuration of compound **2**. The VCD data revealed vibrational transitions at 1154 and 1159 cm^{-1}. In addition, it was assumed that the C−H group bending vibrations at 1307, 1453, and 1455 cm^{-1} primarily originated from the C−O group at the chiral center, C-5. Furthermore, it was evident that the bending vibrations of the C−H group (1307, 1453, and 1455 cm^{-1}) were influenced by the chiral center C-5.[26] By comparing the experimental and calculated VCD data, the absolute configuration of compound **2** was confirmed as (3*R*,5*S*)-2,3,5-trihydroxy-2,6,10,15,19,23-hexamethyl-tetracosa-6,10,14,18,22-pentaene (Figures 2B and 3B).

Compound **3** had the molecular formula $C_{30}H_{52}O_3$ and was obtained as a colorless oil, as determined by its HRESIMS ion peak at *m*/*z* 505.3899 $[M + HCOO]^-$ (calculated for $[C_{31}H_{53}O_5]^-$, 505.3893). ^1H NMR spectroscopic data of compound **3** differed from those of compounds **1** and **2** (Table 1). There were differences in the chemical shifts of five olefinic groups at δ_H 5.23 (H, br t, *J* = 7.0 Hz, H-7), 5.15 (3H, overlapped, H-11, H-14, H-22), and 5.19 (H, br t, *J* = 7.1 Hz, H-18) and two oxygenated methines at δ_H 3.35 (1H, br d, *J* = 10.5 Hz, H-3) and 4.40 (1H, td, *J* = 8.4, 4.6 Hz, H-21), suggesting that the location of the hydroxy group was different. Using the $^1H-^1H$ COSY of H_2-20/H-21/H-22 and the HMBC from H_2-20/Me-29 to C-18/C-19, it was ascertained

https://doi.org/10.1021/acsomega.3c03873
ACS Omega 2023, 8, 32804−32816

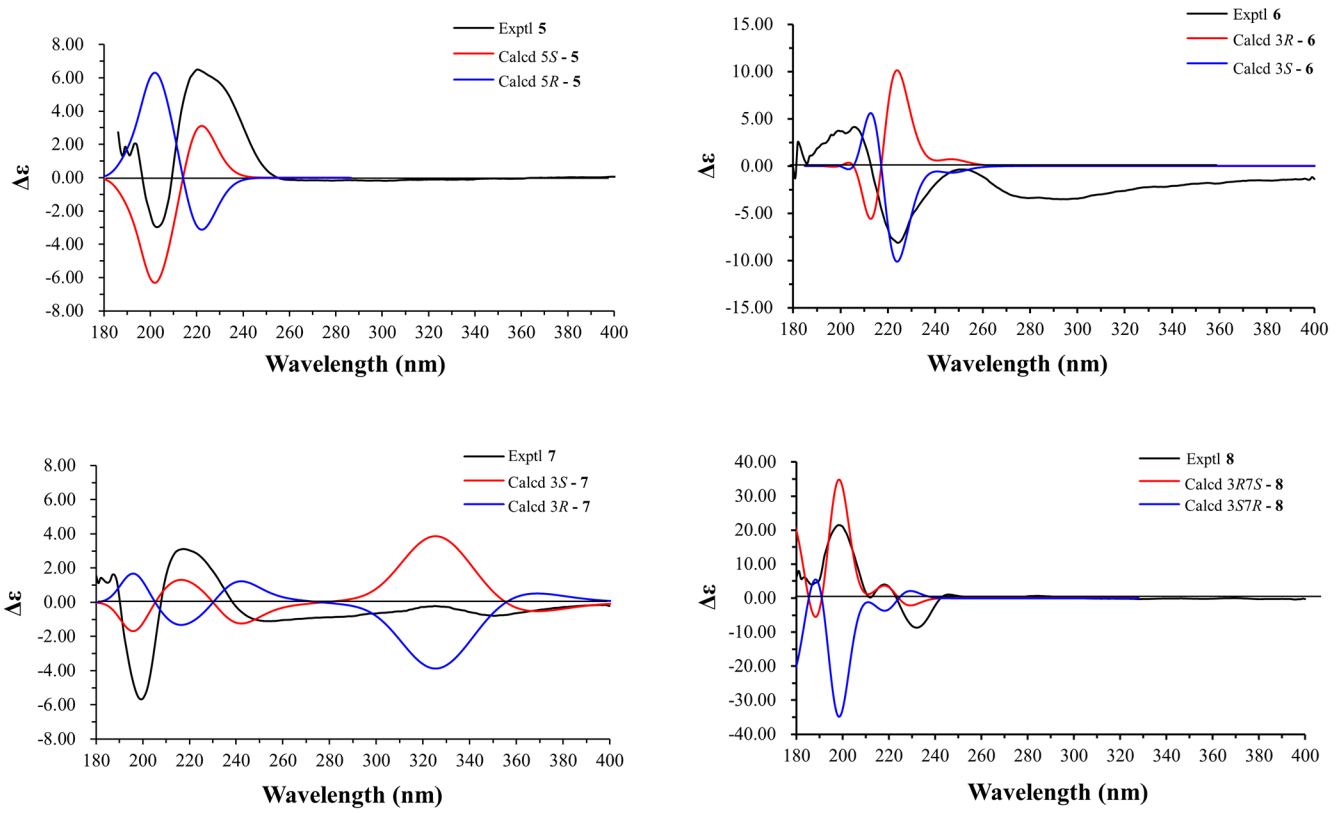

Figure 4. Calculated (red and blue) ECD curves and experimental ECD curves (black) employing a UV correction [shifting = 1 nm (**5**), 15 nm (**6**), −5 nm (**7**) and −18 nm (**8**), sigma/gamma value = 0.28 eV].

that compound **3** was distinct, differing in the location of the hydroxy group (C-21) from compounds **1** and **2**. The connection between units **3a** and **3b** was confirmed by HMBC between H-11 and C-13 (Figure 1). Due to the limited amount of compound **3** available, it was difficult to obtain sufficient VCD data. As a result, the absolute configuration of compound **3** could not be resolved at this time. The structure of compound **3** was proposed to be 2,3,21-trihydroxy-2,6,10,15,19,23-hexamethyl-tetracosa-6,10,14,18,22-pentaene.

Compound **5** was isolated as a colorless oil and had a molecular formula of $C_{15}H_{26}O_2$, as determined by its HRESIMS ion peak at m/z 283.1906 $[M + HCOO]^-$ (calculated for $[C_{16}H_{27}O_4]^-$, 283.1909). The one-hydroxy-bonded methine was different from *trans, trans*-farnesol, which has been isolated from the same source.[27] Using the $^1H-^1H$ COSY of H-3/H_2-4/H-5 and HMBC from H-5/Me-14 to C-6/C-7, it was confirmed that compound **5** was distinct from *trans, trans*-farnesol, differing in the location of a single hydroxy group (C-5). The presence of the three isoprene moieties was verified by comparing the 1D and 2D NMR data, and the connection of each of these moieties was assigned by $^1H-^1H$ and HMBC (Figure 1). The calculated and experimental ECD spectra of compound **5** were compared because of the presence of a chiral carbon in this compound. The experimental ECD spectrum of **5** displayed a negative Cotton effect at 204 nm and a positive Cotton effect at 223 nm, which are consistent with the calculated ECD spectrum of the 5*S* configuration, whereas its enantiomer (5*R*) showed the opposite calculated ECD spectrum (Figure 4). Therefore, the absolute configuration of **5** was established as 5*S* and was determined as 5*S*-hydroxy-*trans, trans*-farnesol. Although compound **5** has been reported previously as a synthetic product, its absolute configuration has not been determined.[28] Thus, this study reports, for the first time, the isolation of naturally occurring compound **5** and determination of its absolute configuration.

The molecular formula of compound **6**, a yellowish oil, was determined as $C_{13}H_{18}O_3$ based on the HRESIMS ion peak at m/z 245.1144 $[M + Na]^+$ (calculated for $[C_{13}H_{18}O_3Na]^+$, 245.1154) with five degrees of unsaturation. The IR spectrum indicated the presence of hydroxyl groups at 3436 cm^{-1} and ester groups at 1733 cm^{-1}. The ^1H NMR spectrum exhibited signals corresponding to five benzene protons at δ_H 7.29 (2H, m, H-2′, H-6′) and δ_H 7.19 (3H, m, H-3′, H-4′, H-5′), one oxygenated methine at δ_H 3.69 (1H, m, H-3), one methyl at δ_H 2.06 (3H, s, H-7), and a series of methylene groups at δ_H 1.72−4.38 (H-1, H-2, H-4, H-5). The ^{13}C NMR, DEPT, and HSQC spectra of compound **6** displayed the presence of 13 carbon signals consisting of one quaternary carbon (one ester carbon at δ_C 171.6, C-6), six benzene carbons at δ_C 141.9 (C-1′), 128.4 (C-2′, C-6′), 128.5 (C-3′, C-5′), and 125.9 (C-4′), one oxygenated methine at δ_C 68.0 (C-3), four methylenes at δ_C 32.0 (C-1), 37.1 (C-2), 36.5 (C-4), and 61.7 (C-5), and one methyl at δ_C 21.0 (C-7). The HMBC from H-2′ to C-1′/C-3′/C-4′/C-6′ and from H_3-7 to C-6 confirmed benzene and acetyl moieties, respectively. With the $^1H-^1H$ COSY cross-peak, which showed the presence of one spin−spin coupling system of H_2-1/H_2-2/H-3/H_2-4/H_2-5, the HMBC from H_2-1 to C-2′ and H_2-5 to C-6 could be assigned to compound **6** (Figure 1). The ECD spectrum of compound **6**, obtained from the experiment, exhibited a negative Cotton effect at 223 nm. These results are in agreement with the calculated ECD

https://doi.org/10.1021/acsomega.3c03873
ACS Omega 2023, 8, 32804−32816

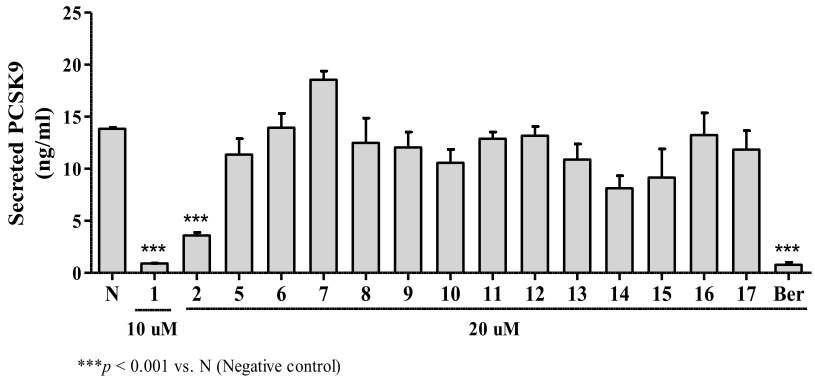

Figure 5. Effects of compounds **1**, **2**, and **5**−**17** on PCSK9 secretion in HepG2 cells. PCSK9 ELISAs were assayed with the medium harvested from compounds treated with an indicated dose and berberine chloride for 24 h. (n = 3, biologically independent samples per group; data presented are mean ± S.E.M.) $^{**}p < 0.01$ and $^{***}p < 0.001$ as compared to the negative control (N) by Dunnett's t-test.

spectrum for the 3*S* configuration. The planar structure was confirmed by comparing it to the reference and establishing it as the same compound.[29] ECD analysis was performed on a single chiral center. The ECD spectrum, obtained by applying UV correction using both the calculated and experimental UV spectra, showed a negative Cotton effect at 223 nm, which aligned with the shifted ECD spectrum after UV correction. Based on this observation, the stereochemistry was determined to be *S*. The enantiomer of compound **6**, 3*R*, displayed the opposite calculated ECD spectrum (Figure 4). Based on these findings, it was concluded that the absolute configuration of compound **6** is 3*S*, and it was further determined to be (*S*)-1-acetoxy-5-phenyl-3-pentanol.

To the best of our knowledge, this is the first time that compound **6** has been derived from a natural product.[29]

Compound **7** was obtained as a yellow powder and possessed a molecular formula of $C_{19}H_{20}O_3$, as determined by its HRESIMS ion peak at m/z 295.1336 $[M - H]^-$ (calculated for $[C_{19}H_{19}O_3]^-$, 295.1334). The ^{1}H NMR and ^{13}C NMR spectra of compound **7** were the same as those of (*R*)-4″-hydroxyyashabushiketol, a class of acyclic diarylheptanoids, which has already been isolated from the same source.[10] Based on the spectroscopic data from the reference, it was confirmed to have the same planar structure. Due to the opposite value of specific optical rotation with (*R*)-4″-hydroxyyashabushiketol, further ECD calculations were conducted. Comparison between the experimental data and the calculated results was carried out to determine the stereochemistry of the single chiral center. UV correction of the ECD spectrum was conducted based on the calculated and experimental UV spectra. Compound **7** exhibited a measured ECD spectrum showing negative Cotton effects at 199, 250, and 327 and 327 nm and positive Cotton effects at 219 and 350 nm. These experimental results aligned with the calculated ECD spectrum for the 3*S* configuration. In contrast, the enantiomer of compound **7**, 3*R*, exhibited a calculated ECD spectrum that was the opposite of that of compound **7** (Figure 4). Based on these observations, it was determined that compound **7** possesses the absolute configuration of 3*S* and was identified as (*S*)-4″-hydroxyyashabushiketol, which is the enantiomer of (*R*)-4″-hydroxyyashabushiketol (Figure 4).

Compound **8** was isolated as a white amorphous powder and had the molecular formula $C_{19}H_{20}O_3$, as determined by its HRESIMS ion peak at m/z 295.1332 $[M - H]^-$ (calculated for $[C_{19}H_{19}O_3]^-$, 295.1334). By comparing 1D and 2D NMR data, the planar structure of compound **8** was found to be the same as that of (3*S*,7*R*)-5,6-dehydro-1,7-bis(4-hydroxyphenyl)-4″-de-*O*-methylcentrolobine, a class of diarylheptanoids, which has already been isolated from the same genus.[30] Based on ECD data, compound **8** displayed an ECD spectrum with negative Cotton effects at 189, 211, and 234 nm and positive Cotton effects at 194 and 219 nm, matching the calculated ECD spectrum for the 3*R* and 7S configuration. Conversely, the enantiomers of compound **8**, 3*S* and 7*R*, exhibited the opposite calculated ECD spectra (Figure 4). These findings led to the conclusion that compound **8** possesses the absolute configuration of 3*R* and 7*S* and was identified as (3*R*,7*S*)-5,6-dehydro-1,7-bis(4-hydroxyphenyl)-4″-de-*O*-methylcentrolobine, which was isolated for the first time from a natural source (Figure 4).[31]

Ten known compounds, including 2,3,5,22,23-pentahydroxy-2,6,10,15,19,23-hexamethyl-tetracosa-6,10,14,18-tetraene (**4**),[17] aniba dimer A (**9**),[32] 6,6′-(3,4-diphenylcyclobutane-1,2-diyl)bis(4-methoxy-2*H*-pyran-2-one) (**10**),[32] dihydro-5,6-dehydrokawain (**11**),[33] 5,6-dehydrokawain (**12**),[33] (3*R*,5*S*)-*trans*-3,5-dihydroxy-1,7-diphenyl-1-heptene (**13**),[27] (3*S*,5*S*)-*trans*-3,5-dihydroxy-1,7-diphenyl-1-heptene (**14**),[27] yashabushidiol A (**15**),[27] (+)-hannokinol (**16**),[34] and *meso*-hannokinol (**17**)[34] were identified by comparing their spectroscopic data to the data obtained from the literature, and all of the 10 known compounds have been previously reported as derived from the *Alpinia* genus.

Before investigating the effects of the isolates on PCSK9, a cell viability test was performed using a WST-8 assay on human HepG2 cells, applying a 20 μM concentration (Figure S85A). The results showed that compounds **3** and **4** caused a significant decrease in cell viability, while compound **1** exhibited slight cytotoxicity compared with the other compounds. Therefore, cell viability tests were conducted using lower concentrations for compounds **1**, **3**, and **4** (Figure S85B−D). Compound **1** did not exhibit significant cytotoxicity using concentrations of 10 μM or lower; thus, 10 μM was selected for further testing. However, compounds **3** and **4** were excluded from any further experiments as they significantly decreased cell viability.

As PCSK9 binds to the LDLR on the cell surface to induce lysosomal degradation, a reduction in PCSK9 secretion is crucial for maintaining cell−surface LDLR for LDL-C uptake. Therefore, the effects of compounds **1**, **2**, and **5**−**17** were examined for their effects on PCSK9 secretion using enzyme linked immunosorbent assays (ELISAs) (Figure 5). Com-

https://doi.org/10.1021/acsomega.3c03873
ACS Omega 2023, 8, 32804−32816

pounds **1** and **2** were shown to block the secretion of PCSK9 from HepG2 cells at the indicated doses. Therefore, compounds **1** and **2** were selected for further investigation.

Compounds **1** and **2** were evaluated for their effects on the expression of PCSK9 and LDLR at both the mRNA and protein levels in human HepG2 cells. At concentrations of 10 and 20 μM, respectively, compounds **1** and **2** significantly downregulated PCSK9 mRNA expression while slightly upregulating LDLR mRNA expression compared to the negative control group (Figure 6). Furthermore, we tested

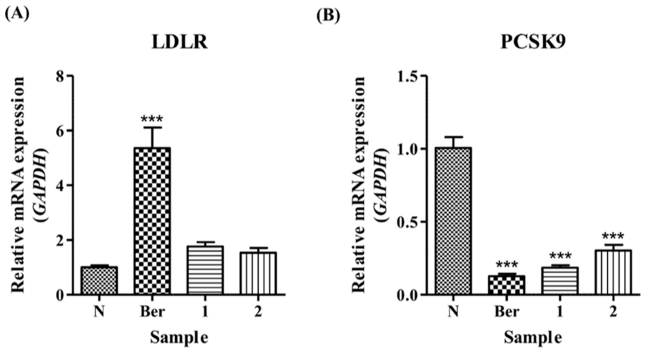

Figure 6. Effects of compounds **1** and **2** on the LDLR and PCSK9 mRNA expressions in the HepG2 cells. (A) The expression of LDLR mRNA was assayed by qRT-PCR in cells treated with compounds **1** (10 μM), **2** (20 μM), and berberine chloride (Ber), the positive control, (20 μM) for 24 h. (B) The expression of PCSK9 mRNA was assayed by qRT-PCR in cells treated with compounds **1** (10 μM), **2** (20 μM), and berberine chloride (Ber), the positive control, (20 μM) for 24 h. (n = 3, biologically independent samples per group; data presented are mean ± S.E.M.) ***p < 0.001 as compared to the negative control (N) by Dunnett's t-test.

compounds **1** and **2** at a range of concentrations (0.625−10 and 1.25−20 μM, respectively) for their inhibition of PCSK9 mRNA expressions in HepG2 cells (Figure S86). We found that compounds **1** and **2** inhibited PCSK9 mRNA expression with the IC_{50} values of 2.94 and 15.08 μM, respectively.

Compounds **1** and **2** did not exhibit cytotoxicity at concentrations of up to 10 and 20 μM, respectively (Figures S85A and S85B). Therefore, concentrations of 5 and 10 μM for compound **1** and of 10 and 20 μM for compound **2** were used to evaluate protein level expressions (Figure 7). Protein expression levels of PCSK9 were reduced when HepG2 cells were treated with compounds **1** and **2**. However, LDLR expression was not upregulated when compared to berberine chloride (positive control), which is the salt form of berberine. Berberine inhibits hepatic nuclear factor 1 alpha (HNF1α), which is known as a PCSK9 *trans*-activator. This results in the downregulation of PCSK9 mRNA expression.[35] In addition, berberine regulates LDLR expression post-transcriptionally by facilitating the stabilization of LDLR mRNA.[36] Berberine therefore lowers both PCSK9 mRNA and protein expressions and maintains high expression of both LDLR mRNA and protein. Compounds **1** and **2** showed contrasting results to berberine chloride, suggesting that different mechanisms are involved for these compounds.

To evaluate the concentration-dependent inhibition of PCSK9 secretion by compounds **1** and **2**, further experiments were conducted over a range of concentrations (Figure 8). Both compounds exhibited a dose-dependent reduction in PCSK9 secretion, with compound **1** demonstrating a significant decrease in PCSK9 secretion at concentrations of 5 and 10 μM and compound **2** displaying a significant decrease in PCSK9 secretion at a concentration of 20 μM.

Additionally, in respect of the established "Lipinski's rule of five" for pharmaceutical candidates,[37] the lipophilicity values of the compounds were calculated (Table S9). Lipinski's rules were established based on an analysis of the physicochemical properties of orally active drugs,[38] so it could be a good parameter for selecting drug candidates. According to this calculation, compounds with log P values of 5 or below, which have moderate lipophilicity, were found to be compounds **5**−**10**, **16**, and **17**. However, as observed in previous biological experiments, the active compounds were compounds **1** and **2**, which had relatively higher log P values (7.7958 and 8.4518, respectively). These compounds have log P values above 5, indicating high lipophilicity. According to Lipinski's rule, compounds with high lipophilicity are generally not considered ideal drug candidates because they can have, for example, low water solubility, limited cell membrane permeability, and metabolic concerns. However, despite these drawbacks, compounds **1** and **2** showed promising PCSK9 inhibitory effects. If further research, such as structural modifications, can find a way to reduce lipophilicity while maintaining the efficacy, they may have the potential to become better drugs with an improved c log P value.

CONCLUSIONS

In conclusion, 17 compounds were isolated from the methanolic extracts of *Alpina Katsumadai* seeds. Their structures were determined through various physicochemical and spectroscopic methods. All absolute configurations of isolated new compounds were determined using VCD and ECD. Especially, the absolute configurations of compounds **1** and **2** were identified by comparing the calculated and experimental VCD data as the ECD method was unable to distinguish the diastereomers. The structures of the known compounds were elucidated using various spectroscopic methods, confirming their planar structures. For compounds with known planar stereochemistry, the structures were determined by comparing them with previous references. The absolute configuration of compounds was determined by comparing the experimental ECD spectrum with the calculated ECD spectrum, considering the UV correction value obtained from the comparison of the calculated and experimental UV spectra. Of the isolates, compounds **1** and **2**, two new compounds, downregulated PCSK9 in both mRNA and protein levels, with a particular emphasis on compound **1**. Compound **1** exhibited inhibition of PCSK9 to a similar extent to that of the positive control, berberine chloride. While further investigation is required for the underlying mechanism, compound **1** has demonstrated promising potential as an inhibitor of PCSK9. Additionally, we calculated the c log P values to assess the drug-likeness aspect based on Lipinski's rule. Both compounds **1** and **2** exhibited values beyond the desirable range, and this suggests that further research on the modification of these compounds is warranted in order to develop these compounds as drugs.

MATERIALS AND METHODS

Materials. Column chromatography was conducted on silica gel (particle size: 40−60 μm, 230−400 mesh, Merck, Darmstadt, Germany). Medium-pressure liquid chromatog-

https://doi.org/10.1021/acsomega.3c03873
ACS Omega 2023, 8, 32804−32816

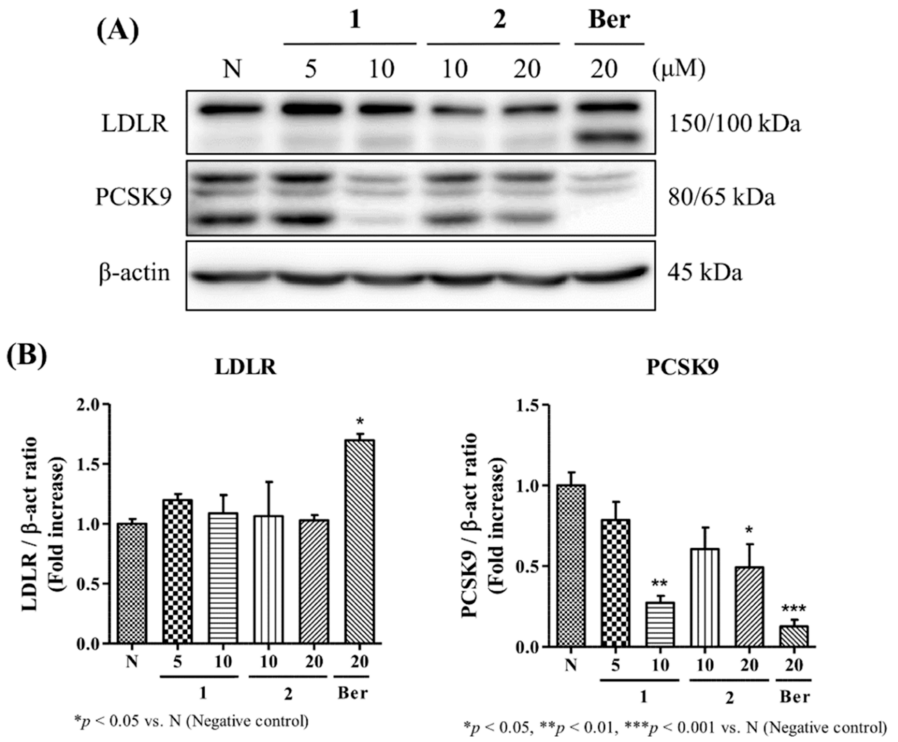

Figure 7. (A) Effects of **1** and **2** on LDLR, PCSK9, and β−actin protein expression in HepG2 cells. HepG2 cells were treated with indicated concentrations and berberine chloride (Ber) for 24h. The expressions of the proteins were examined by Western blot analysis. (B) Immunoblot signals were quantified by using ImageJ software (NIH, Bethesda, MD). (n = 3, biologically independent samples per group; data presented are mean ± S.E.M.) *p < 0.05, **p < 0.01, and ***p < 0.001 as compared to the negative control (N) by Dunnett's t-test.

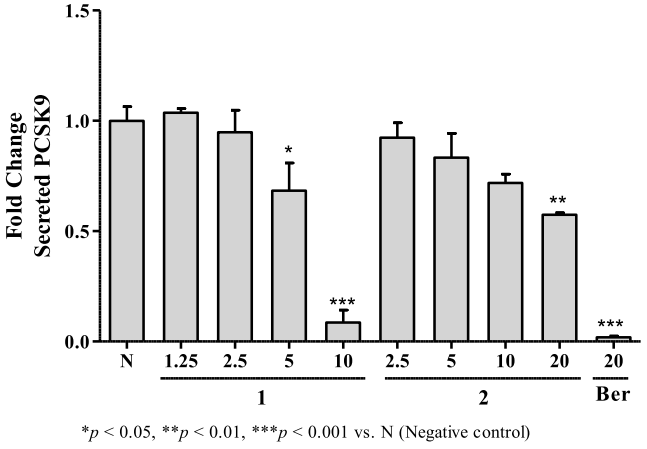

Figure 8. Effects of compounds **1** and **2** on PCSK9 secretion in the concentration range in HepG2 cells. PCSK9 ELISAs were assayed in the medium harvested from compounds **1** and **2** treated with an increasing dose and berberine chloride (Ber) for 24 h. (n = 3, biologically independent samples per group; data presented are mean ± S.E.M.) *p < 0.05, **p < 0.01, and ***p < 0.001 as compared to the negative control (N) by Dunnett's t-test.

raphy (MPLC) was performed on a Biotage Isolera One (Biotage, Uppsala, Sweden) with C18 RP silica gel (Cosmosil, Kyoto, Japan). High-performance liquid chromatography (HPLC) was performed with a Gilson 321 pump and a Gilson 172 diode array detector (Gilson, Madison, WI, USA), with the aid of two columns; Luna, C18 [S-5 μm, 250 × 10 mm] (Phenomenex, CA, USA), YMC-J'sphere ODS-M80, HPLC column [S-5 μm, 250 × 10 mm] (YMC, Kyoto, Japan) and YMC-Triart Phenyl, HPLC column [S-5 μm, 250 × 10 mm] (YMC, Kyoto, Japan). Mass spectral data were measured using a Waters Xevo G2 Q-TOF mass spectrometer, UHPLC-ESI-QTOF-MS (Waters, Medford, MA, USA). Nuclear magnetic resonance (NMR) spectra were recorded using JNM-ECA AVANCE 400 and 600 MHz spectrometers (JEOL Ltd., Tokyo, Japan) and a Bruker AVANCE 500 MHz spectrometer (Bruker, Karlsruhe, Germany). Circular dichroism and ultraviolet−visible spectra were measured by a Chirascan-Plus ECD spectrometer (Applied Photophysics Ltd., Tokyo, Japan). A JASCO P-2000 digital polarimeter (JASCO, Tokyo, Japan) was used to measure optical rotation. Fourier transform infrared spectroscopy (JASCO, FT/IR-4200, FT/IR-4700, Tokyo, Japan) was used to measure IR spectra. VCD and IR spectra were measured by Chiral*IR*-2X (Biotools, Inc., Jupiter, USA). Thin layer chromatography (TLC) analysis was performed on silica gel 60 F_{254} and silica gel RP-C_{18} plates (Merck, Darmstadt, Germany). The spots were visualized by spraying 10% H_2SO_4. Purified water was obtained using a Milli-Q system (Waters Corporation, Milford, MA, USA).

Reagents. Solvents for extraction and isolation including methanol, *n*-hexane, chloroform, EtOAc, *n*-butanol, acetonitrile (CH_3CN, HPLC grade), and methanol (MeOH, HPLC grade) were purchased from SK chemical (Seoul, Korea). Solvents for NMR spectroscopy ($CDCl_3$ and MeOH) were purchased from Cambridge Isotope Laboratories, Inc. (Andover, MA).

Plant Material. The dried seeds of *A. katsumadai*, originating from Vietnam, were purchased from a Korean market E-Pul-Ip-Jeyak in February 2019 and were identified by Kwangmyeong Raw Medicine Co., Ltd. A voucher specimen (Voucher no. CYWSNU-KP0024) was deposited at the College of Pharmacy, Seoul National University, Republic of Korea.

https://doi.org/10.1021/acsomega.3c03873
ACS Omega 2023, 8, 32804−32816

Methods. *Extraction and Isolation.* Dried seeds of *A. katsumadai* (4.8 kg) were extracted with 6 L of MeOH at room temperature (3 days × 5 times). The solvent was evaporated in vacuo at 39 °C, and the crude extract (482.0 g) was suspended in H_2O (1.5 L) for partition with *n*-hexane (3 × 1.5 L), $CHCl_3$ (3 × 1.5 L), EtOAc (3 × 1.5 L), and *n*-butanol (3 × 1.5 L) successively. The *n*-hexane part (33.0 g) was subjected to silica gel column chromatography (CC) using a gradient solvent system, from *n*-hexane/EtOAc (80:1 → 1:1) to $CHCl_3$/MeOH (10:1 → 1:1), to afford 17 fractions (F1−F17). Of these subfractions, subfractions 12 and 13 + 14 were found to be active (Figure S84). F12 (1.5 g) was subjected to a reversed-phase MPLC eluted with a MeOH/H_2O (30:70 → 100:0) gradient solvent system to afford 30 (F12−1 to F12−30) subfractions. F12−2 (20.8 mg) was separated by semipreparative HPLC (YMC-Triart C18, 250 × 10 mm, 50−65% MeOH in H_2O containing 0.1% formic acid, 3 mL/min) to yield **16** (3.6 mg, t_R 16.5 min), **6** (3.6 mg, t_R 32.6 min), and **11** (1.5 mg, t_R 41.5 min). F12−4 (22.7 mg) was subjected to semipreparative HPLC (YMC-Triart C18, 250 × 10 mm, 70−80% MeOH in H_2O containing 0.1% formic acid, 3 mL/min) to afford **8** (3.0 mg, t_R 11.5 min), **12** (10.1 mg, t_R 14.7 min), **9** (2.0 mg, t_R 23.1 min), and **10** (3.7 mg, t_R 24.6 min). A part of F12−6 (50 mg) was subjected to semipreparative HPLC (YMC-Triart C18, 250 × 10 mm, 65% MeOH in H_2O containing 0.1% formic acid, 3 mL/min) to yield **13** (5.2 mg, t_R 31.5 min), **14** (20.1 mg, t_R 33.3 min), and **15** (14.7 mg, t_R 41.5 min). **4** (13.2 mg, t_R 59.2 min) and **17** (3.6 mg, t_R 78.5 min) were obtained using semipreparative HPLC (YMC-Triart C18, 250 × 10 mm, 65−74.5% MeOH in H_2O containing 0.1% formic acid, 3 mL/min). F13 and F14 were pooled together for Sephadex LH-20 CC (454.0 mg) using MeOH/H_2O (20:1) to yield 38 subfractions. F13,14−9 and F13,14−10 were pooled together (93.4 mg) and subjected to semipreparative HPLC (YMC-J'SPHERE ODS H80, 250 × 10 mm, 95% CH_3CN in H_2O containing 0.1% formic acid, 3 mL/min) to obtain **1** (2.0 mg, t_R 15.6 min) and **2** (53.0 mg, t_R 28.1 min). F13,14−11 (84.8 mg) was separated using semipreparative HPLC (YMC-Triart C18, 250 × 10 mm, 95−100% CH_3CN in H_2O containing 0.1% formic acid, 3 mL/min) to afford **3** (3.4 mg, t_R 51.9 min). **5** (4.8 mg, t_R 13.3 min) was isolated from F13,14−13 and F13,14−14 using semipreparative HPLC (YMC-Triart C18, 250 × 10 mm, 75% MeOH in H_2O containing 0.1% formic acid, 3 mL/min). F13,14−23, F13,14−24, and F13,14−25 were pooled together for semipreparative HPLC (YMC-Triart C18, 250 × 10 mm, 60% MeOH in H_2O containing 0.1% formic acid, 3 mL/min) to yield **7** (1.5 mg, t_R 31.5 min).

Structural analysis of all isolated compounds was conducted according to the procedures outlined in our previous study for structural elucidation.[15,16]

*(3R,20S)-2,3,20-Trihydroxy-2,6,10,15,19,23-hexamethyltetracosa-6,10,14,18,22-Pentaene (**1**).* Colorless oil; $[\alpha]_D^{20}$ + 70.0 (*c* 0.4, MeOH); UV (MeOH) λ_{max} (log ε) 202 (4.23) nm; ECD (MeOH) λ_{max} ($\Delta\varepsilon$) 215 (+2.27) nm; IR (neat) ν_{max}: 3393, 2924, 2857, 1738, 1671, 1561, 1518, 1444, 1375, 1247, 1164, 1085, 1020 cm^{-1}; ^1H and ^{13}C NMR ($CDCl_3$), see Table 1; HRESIMS *m*/*z*: $[M + Na]^+$ 483.3814 (calcd for $[C_{30}H_{52}O_3Na]^+$, 483.3814).

*(3R,5S)-2,3,5-Trihydroxy-2,6,10,15,19,23-hexamethyltetracosa-6,10,14,18,22-Pentaene (**2**).* Colorless oil; $[\alpha]_D^{20}$ + 38.8 (*c* 0.8, MeOH); UV (MeOH) λ_{max} (log ε) 204 (4.43) nm; ECD (MeOH) λ_{max} ($\Delta\varepsilon$) 210 (+1.57) nm; IR (neat) ν_{max}: 3380, 2969, 2922, 2858, 1443, 1376, 1157, 1083, 858 cm^{-1}; ^1H and ^{13}C NMR ($CDCl_3$), see Table 1; HRESIMS *m*/*z*: $[M + HCOO]^-$ 505.3891 (calcd for $[C_{31}H_{53}O_5]^-$, 505.3893).

*2,3,21-Trihydroxy-2,6,10,15,19,23-hexamethyl-tetracosa-6,10,14,18,22-pentaene (**3**).* Colorless oil; $[\alpha]_D^{20}$ + 8.4 (*c* 0.3, MeOH); UV (MeOH) λ_{max} (log ε) 201 (4.33) nm; ECD (MeOH) λ_{max} ($\Delta\varepsilon$) 213 (−0.82) nm; IR (neat) ν_{max}: 3357, 3349, 2951, 2856, 2845, 1706, 1668, 1629, 1611, 1443, 1389, 1386 cm^{-1}; ^1H and ^{13}C NMR ($CDCl_3$), see Table 1; HRESIMS *m*/*z*: $[M + HCOO]^-$ 505.3899 (calcd for $[C_{31}H_{53}O_5]^-$, 505.3893).

*(S)-5-Hydroxy-trans,trans-farnesol (**5**).* Colorless oil; $[\alpha]_D^{20}$ + 75.9 (*c* 0.4, MeOH); UV (MeOH) λ_{max} (log ε) 201 (4.22) nm; ECD (MeOH) λ_{max} ($\Delta\varepsilon$) 214 (+1.81) nm; IR (neat) ν_{max}: 3411, 2973, 2925, 2279, 1753, 1638, 1456, 1380, 1301, 1162, 1102, 1037, 896, 817, 661 cm^{-1}; ^1H NMR ($CDCl_3$, 600 MHz): δ 5.41 (1H, m, H-11), 5.38 (1H, m, H-7), 5.09 (1H, m, H-3), 4.15 (2H, br d, *J* = 6.9 Hz, H-12), 3.98 (H, br dd, *J* = 7.9, 5.4 Hz, H-5), 2.29 (1H, overlapped, H-4a), 2.21 (1H, m, H-4b), 2.16 (2H, overlapped, H-8), 2.08 (2H, overlapped, H-9), 1.72 (3H, s, H-1), 1.64 (3H, s, H-13), 1.62 (6H, s, H-14, H-15); ^{13}C NMR ($CDCl_3$, 150 MHz): δ 139.3 (C, C-10), 137.1 (C, C-6), 134.8 (C, C-2), 125.7 (CH, C-7), 123.7 (CH, C-11), 120.1 (CH, C-3), 77.2 (CH, C-5), 59.4 (CH_2, C-12), 39.1 (CH_2, C-9), 34.2 (CH_2, C-4), 25.9 (CH_3, C-1), 25.7 (CH_2, C-8), 18.0 (CH_3, C-13), 16.2 (CH_3, C-15), 11.7 (CH_3, C-14); HRESIMS *m*/*z*: $[M + HCOO]^-$ 283.1906 (calcd for $[C_{16}H_{27}O_4]^-$, 283.1909).

*(S)-1-Acetoxy-5-phenyl-3-pentanol (**6**).* Yellowish oil; $[\alpha]_D^{20}$ − 20.5 (*c* 0.1, MeOH); UV (MeOH) λ_{max} (log ε) 199 (4.10), 252 (3.03) nm; ECD (MeOH) λ_{max} ($\Delta\varepsilon$) 206 (+0.10), 224 (−0.20), 252 (0.00), 293 (−0.09) nm; IR (neat) ν_{max}: 3437, 2925, 2858, 1734, 1602, 1369, 1242, 1046 cm^{-1}; ^1H NMR ($CDCl_3$, 400 MHz): δ 7.29 (2H, m, H-2′, H-6′), 7.19 (3H, m, H-3′, H-4′, H-5′), 4.38 (1H, dt, *J* = 11.2, 5.5 Hz, H-5a), 3.69 (1H, m, H-3), 2.81 (2H, ddd, *J* = 11.3, 8.7, 5.0 Hz, H-1a, H-5b), 2.68 (1H, m, H-1b), 2.06 (3H, s, H-7) 1.88 (1H, overlapped, H-4a), 1.80 (2H, overlapped, H-2), 1.72 (H, overlapped, H-4b); ^{13}C NMR ($CDCl_3$, 100 MHz): δ 171.6 (C, C-6), 141.9 (C, C-1′), 128.5 (CH, C-3′, C-5′), 128.4 (CH, C-2′, C-6′), 125.9 (CH, C-4′), 68.0 (CH, C-3), 61.7 (CH_2, C-5), 37.1 (CH_2, C-2), 36.5 (CH_2, C-4), 32.0 (CH_2, C-1), 21.0 (CH_3, C-7); HRESIMS *m*/*z*: $[M + Na]^+$ 245.1144 (calcd for $[C_{13}H_{18}O_3Na]^+$, 245.1154).

*(S)-4″-Hydroxyyashabushiketol (**7**).* Yellow powder; $[\alpha]_D^{20}$ + 82.9 (*c* 0.3, MeOH); UV (MeOH) λ_{max} (log ε) 201 (4.02), 236 (3.87), 326 (4.32) nm; ECD (MeOH) λ_{max} ($\Delta\varepsilon$) 218 (+0.62), 255 (−0.22), 325 (−0.04), 351 (−0.16) nm; ^1H NMR ($CDCl_3$, 500 MHz): δ 7.50 (1H, d, *J* = 16.0, H-7), 7.45 (2H, d, *J* = 8.6, H-2″, H-6″), 7.29 (2H, m, H-3′, H-5′), 7.22 (2H, m, H-2′, H-6′), 7.18 (1H, m, H-4′), 6.86 (2H, d, *J* = 8.7, H-3′′, H-5′′), 6.58 (1H, d, *J* = 16.1, H-6), 4.15 (1H, m, H-3), 2.88 (1H, m, H-1a), 2.84 (1H, m, H-4a), 2.78 (1H, m, H-4b), 2.73 (1H, m, H-1b), 1.90 (1H, m, H-2a), 1.77 (1H, m, H-2b); ^{13}C NMR ($CDCl_3$, 125 MHz): δ 200.9 (C, C-5), 158.2 (C, C-4″), 143.5 (CH, C-7), 141.9 (C, C-1′), 130.5 (CH, C-2″, C-6″), 128.5 (CH, C-2′, C-6′), 128.4 (CH, C-3′, C-5′), 127.0 (C, C-1″), 125.9 (CH, C-4′), 124.1 (CH, C-6), 67.3 (CH, C-3), 46.6 (CH_2, C-4), 38.2 (CH_2, C-2), 31.8 (CH_2, C-1); HRESIMS *m*/*z*: $[M - H]^-$ 437.1616 (calcd for $[C_{19}H_{19}O_3]^-$, 437.1606).

*(3R,7S)-5,6-Dehydro-1,7-bis(4-hydroxyphenyl)-4″-de-O-methylcentrolobine (**8**).* Yellow powder; $[\alpha]_D^{20}$ + 107.0 (*c* 0.1,

https://doi.org/10.1021/acsomega.3c03873
ACS Omega 2023, 8, 32804−32816

MeOH); UV (MeOH) λ_{max} (log ε) 199 (4.46), 226 (4.07), 278 (3.50) nm; ECD (MeOH) λ_{max} ($\Delta\varepsilon$) 200 (+4.97), 212 (+0.06), 218 (+0.97), 232 (−2.04) nm; ^{1}H NMR ($CDCl_3$, 400 MHz): δ 7.29 (2H, d, J = 8.2, H-2″, H-6″), 6.84 (2H, d, J = 8.6, H-3′′, H-5′′), 6.71 (2H, J = 8.5, H-2′, H-6′), 6.60 (2H, J = 8.5, H-3′, H-5′), 6.02−5.94 (1H, m, H-6), 5.23 (1H, m, H-7), 3.45 (2H, tt, J = 9.4, 3.6, H-4), 2.60 (1H, ddd, J = 13.5, 8.2, 5.0, H-1a), 2.42 (1H, dt, J = 13.8, 8.2, H-1b), 2.05 (1H, m, H-5a), 1.97 (1H, m, H-5b), 1.78 (1H, m, H-3), 1.61 (2H, overlapped, H-2); ^{13}C NMR ($CDCl_3$, 100 MHz): δ 155.2 (C, C-4″), 153.3 (C, C-4′), 134.2 (C, C-1′), 133.4 (C, C-1″), 130.2 (CH, C-2″, C-6″), 129.6 (CH, C-2′, C-6′), 127.5 (CH, C-6), 126.1 (CH, C-5), 115.0 (CH, C-3′′, C-5′′), 114.9 (CH, C-3′, C-5′), 73.8 (CH, C-7), 65.5 (CH, C-3), 37.6 (CH_2, C-2), 31.2 (CH_2, C-4), 30.5 (CH_2, C-1); HRESIMS m/z: $[M - H]^-$ 295.1332 (calcd for $[C_{19}H_{19}O_3]^-$, 295.1334).

ECD Calculation. Compounds **1** and **2** were subjected to conformational searches using the GMMX program in Gaussian 16 software after their minimized structures were generated in ChemBio3D Ultra 13.03. Similarly, the minimized structures of compounds **5**, **6**, **7**, and **8** were used for conformational searches in the Spartan 16 program. Both Gaussian 16 and Spartan 16 software were employed for the conformational searches, utilizing MMFF94 molecular force-field calculations for all compounds. Among the generated conformers, several conformers that were expected to exhibit population above 95% were selected, and these were subjected to optimization and frequency calculation, using DFT calculation at the mPW1PW91/6-31+G (d, p) basis set with the CPCM model, using Gaussian 16 software (Gaussian Inc., Wallingford, CT, USA). The solvent model used in this study was methanol. After optimization, the ECD spectra of the optimized conformers were calculated using time-dependent DFT (TDDFT) at the same condition with optimization, with the consideration of the first 10 excitations for **1**, **2**, and **5** and first 20 excitations for **6**, **7**, and **8**. For compounds **1** and **2**, the mPW1PW91/6-31+G(d, p) basis set was initially employed but proved to be insufficient to distinguish diastereomers. Therefore, additional experiments were conducted using the B3LYP/6-31+G(d, p) basis set. The optimization and frequency calculation processes were carried out as previously described. Subsequently, the ECD spectra of the optimized conformers for compounds **1** and **2** were calculated using TDDFT under the same optimization conditions. This calculation considered the first 50 excitations and 3 root values. The overall calculated ECD curves were weighted using Boltzmann factors, which were determined from the Gibbs free energy calculations. The ECD spectra obtained from their relative free energy values were then combined and adjusted for sigma/gamma values and UV correction using the SpecDis 1.70.1 software.[39,40] [shifting = −8 nm (**1** and **2**), 1 nm (**5**), 15 nm (**6**), −5 nm (**7**) and −18 nm (**8**), sigma/gamma value = 0.28 eV] Finally, these calculated ECD spectra were compared to the experimental values.

VCD Calculation. All minimized structures were generated using ChemBio3D Ultra 13.03 and then submitted in the GMMX program in Gaussian 16 software (Gaussian Inc., Wallingford, CT, USA) for conformational searches by using MMFF94 molecular force-field calculations. All conformers were subjected to low level optimization using DFT calculation at the APFD/6-31G (d) basis set with the SCRF model. The solvent model utilized in this study was methanol. Among the generated conformers, several conformers were selected with energies less than 4 kcal/mol from the lowest energy structure for high level optimization using DFT calculation at the APFD/6-311+G (2d, p) basis set with the SCRF model. After high level optimization, the conformers that have energies less than 2.5 kcal/mol from the lowest energy structures were selected for VCD frequency calculation at the same condition with high level optimization. The overall calculated VCD curves were weighted using Boltzmann factors, which were determined from the Gibbs free energy calculations. The VCD spectra obtained from their relative free energy values were then combined and adjusted for gamma values and wave-number correction using the SpecDis 1.70.1 software.[39,40] [shifting = −30 cm^{-1} (**1**) and −35 cm^{-1} (**2**), gamma value = 0.8 cm^{-1}, respectively]. Finally, these calculated VCD spectra were compared to the experimental values.

VCD Measurement. The experimental IR and VCD spectra were obtained for a 0.05 M solution of compound **1** and a 0.1 M solution of compound **2** in $CDCl_3$, using a Chiral*IR*-2X FT-VCD spectrometer (Biotools, Jupiter, FL). The spectrometer was set at a resolution of 4 cm^{-1} and the collection times of 40 and 20 h, respectively. Compounds **1** and **2** were measured in two photoelastic modulator (PEM) modes, set at 1400 cm^{-1}. In order to increase the baseline stability and signal-to-noise ratio, VCD measurements were performed in the dual-PEM mode. This method involves introducing a second PEM after the sample cell with axes parallel to those of the first PEM, allowing for the measurement of VCD using two PEMs. The spectra were calibrated automatically using the standard calibration files. The phase calibration file, '14PHA4WN,' and the VCD intensity calibration file, '14QWP4WN,' obtained from BioTools, were utilized for calibration. These files were designed for an instrument resolution of 4 cm^{-1} and a PEM setting of 1400 cm^{-1}. The VCD spectra of compounds **1** and **2** were obtained with the [Sample] − [Background] spectra process. In the process, the VCD spectrum of the solvent, measured under the same conditions as those for samples, was subtracted from compound **1** and **2** spectra. The VCD spectra were recorded in a SL-4 cell with BaF_2 windows, with 100 μm diameters. All obtained VCD spectra were processed using GRAMS/AI software (ThermoFisher Scientific, USA). The axis values of VCD were defined in terms of molar absorptivity (ε) for both calculated and experimental VCD spectra. These values were determined using the following parameters: b, which represents the path length in centimeters; c, corresponding to the concentration in moles per liter; and (ee), which denotes the enantiomeric excess of the sample.

$$\Delta\varepsilon(\nu) = \Delta A(\nu)/(\mathrm{ee})bc$$

Cell Culture. The HepG2 human hepatocellular liver cell line was obtained from the Korea Research Institute of Bioscience and Biotechnology (South Korea) and grown in modified Eagle's medium (MEM) with Earle's balanced salt solution (EBSS) containing 10% fetal bovine serum and 100 U/mL penicillin/streptomycin sulfate. Cells were incubated in a humidified 5% w/v CO_2 atmosphere at 37 °C. MEM/EBSS, penicillin/streptomycin, and FBS were purchased from Hyclone (Logan, USA).

Cell Viability Tests. Cell viability test was performed with a WST plus-8 kit (GenDEPOT, USA) according to the manufacturer's instructions. Briefly, 5 × 10^3 human HepG2 cells were seeded in a 96-well culture plate on the day before sample treatment. The compounds dissolved in DMSO were

https://doi.org/10.1021/acsomega.3c03873
ACS Omega 2023, 8, 32804−32816

diluted to a concentration from 2.5 to 20 μM in MEM/EBSS without FBS for serum starvation. After treatment, cells were incubated for 24 h for the WST-8 cell viability test.

ELISAs. Secreted PCSK9 levels in culture medium of cells were measured using Human Proprotein Convertase 9/PCSK9 ELISA kits (RayBiotech, USA) in accordance with the manufacturer's instructions. Briefly, 5×10^5 human HepG2 cells were seeded in a 12-well culture plate on the day before the treatment. The compounds dissolved in DMSO were diluted to the indicated concentration in DMEM without FBS. After treatment, cells were incubated for 24 h, and the culture medium was harvested for PCSK9 secretion ELISA. Color development at 450 nm was then measured using an automated microplate ELISA reader. In addition, a standard curve was generated for each assay plate by measuring the absorbance of serial dilutions of recombinant human PCSK9 at 450 nm.

Quantitative Real-time PCR. Total RNA was extracted from HepG2 treated with compounds using TRI Reagent (Genbiotech) according to the manufacturer's instructions. The complementary DNA (cDNA) was synthesized from total RNA using the Maxima First Strand cDNA Synthesis Kit (ThermoFisher Scientific, USA). Real-time PCR for mRNA quantification was performed with a TB Green Premix Ex *Taq*II (TaKaRa Biotechnology, China). The mRNA expression was normalized to the GAPDH and calculated using the $2^{-\Delta\Delta Ct}$ method. The human primers used were the following (5′ to 3′): GAPDH: GTCTCCTCTGACTTCAACAGCG (forward), ACCACCCTGTTGCTGTAGCCAA (reverse); LDLR: GTGCTCCTCGTCTTCCTTTG (forward), TAGCTGTAGCCGTCCTGGTT (reverse), PCSK9: GACACCAGCATACAGAGTGAC (forward) and GTGCCATGACTGTCACACTTGC (reverse). Gene-specific primers were custom-synthesized by Bioneer (Daejeon, Korea).

Western Blot. HepG2 cells were lysed in RIPA buffer containing Pierce Protease and Phosphatase Inhibitor Mini Tablets (ThermoFisher Scientific, USA) on ice for 10 min. Cell lysates were centrifuged at 14,000 rpm for 15 min at 4 °C, and supernatants were quantified using the protein assay reagents A and B (Bio-Rad, USA). Proteins were separated by electrophoresis on a 10% sodium dodecyl sulfate polyacrylamide gel (SDS-PAGE) and were transferred onto a polyvinylidene difluoride (PVDF) membrane. The membrane was treated with 5% skim milk for 1 h and incubated overnight at 4 °C with primary antibodies in 3% bovine serum albumin (BSA). After washing with Tris-buffered saline with 0.1% Tween 20 (TBST), the membrane was incubated with the HRP-conjugated secondary antibody (1:5000) for 1 h at room temperature. The band images were acquired using a ChemiDoc Imaging system (Bio-Rad, USA) using the SuperSignal West Pico PLUS Chemiluminescent Substrate (ThermoFisher Scientific, USA) or Immobilon Western Chemiliminescent HRP Substrate (Millipore, USA).

Statistical Analysis. The results of the experiments are reported as the average value with the standard error of the mean (SEM). We assessed the statistical significance using one-way analysis of variance (ANOVA) and Dunnett's *t*-test for making multiple comparisons. P values below 0.05 were considered significant.

■ ASSOCIATED CONTENT

Supporting Information

The Supporting Information is available free of charge at https://pubs.acs.org/doi/10.1021/acsomega.3c03873.

The Supporting Information is available free of charge on the ACS Publications Web site. Figures for mass spectra and experimental and calculated VCD, ECD, UV, IR, and NMR spectra of **1**, **2**, **3**, **5**, **6**, **7**, and **8** (PDF)

■ AUTHOR INFORMATION

Corresponding Author

Young-Won Chin − *College of Pharmacy and Research Institute of Pharmaceutical Sciences, Seoul National University, Seoul 08826, Republic of Korea;* orcid.org/0000-0001-6964-1779; Phone: +82-2-880-7859; Email: ywchin@snu.ac.kr

Authors

Chae-Yeong An − *College of Pharmacy and Research Institute of Pharmaceutical Sciences, Seoul National University, Seoul 08826, Republic of Korea*

Min-Gyung Son − *College of Pharmacy and Research Institute of Pharmaceutical Sciences, Seoul National University, Seoul 08826, Republic of Korea*

Complete contact information is available at: https://pubs.acs.org/10.1021/acsomega.3c03873

Notes

The authors declare no competing financial interest.

■ ACKNOWLEDGMENTS

This work was supported by a grant (NRF-2022R1A2C1010084) from the National Research Foundation of Korea (NRF) funded by the Korean government (MSIT). This work was also supported by the National Supercomputing Center with supercomputing resources including technical support.

■ REFERENCES

(1) Maxfield, F. R.; Tabas, I. Role of cholesterol and lipid organization in disease. *Nature* **2005**, *438* (7068), 612−621.

(2) Pfrieger, F. Cholesterol homeostasis and function in neurons of the central nervous system. *Cell. Mol. Life Sci.* **2003**, *60*, 1158−1171.

(3) Helkin, A.; Stein, J. J.; Lin, S.; Siddiqui, S.; Maier, K. G.; Gahtan, V. Dyslipidemia part 1—review of lipid metabolism and vascular cell physiology. *Vasc. Endovasc. Surg.* **2016**, *50* (2), 107−118.

(4) Lagace, T. A. PCSK9 and LDLR degradation: regulatory mechanisms in circulation and in cells. *Curr. Opin. Lipidol.* **2014**, *25* (5), 387−393.

(5) Peterson, A. S.; Fong, L. G.; Young, S. G. Errata. PCSK9 function and physiology. *J. Lipid Res.* **2008**, *49* (7), 1595−1599.

(6) Arnold, N.; Koenig, W. PCSK9 Inhibitor Wars: How Does Inclisiran Fit in with Current Monoclonal Antibody Inhibitor Therapy? Considerations for Patient Selection. *Curr. Cardiol. Rep.* **2022**, *24*, 1657−1667.

(7) Gouni-Berthold, I.; Berthold, H. K. PCSK9 antibodies for the treatment of hypercholesterolemia. *Nutrients* **2014**, *6* (12), 5517−5533.

(8) Ruotsalainen, A.-K.; Mäkinen, P.; Ylä-Herttuala, S. Novel RNAi-based therapies for atherosclerosis. *Curr. Atheroscler. Rep.* **2021**, *23* (8), 45.

(9) He, X. F.; Chen, J. J.; Li, T. Z.; Hu, J.; Huang, X. Y.; Zhang, X. M.; Guo, Y. Q.; Geng, C. A. Diarylheptanoid-flavanone Hybrids as

Multiple-target Antidiabetic Agents from Alpinia katsumadai. *Chin. J. Chem.* **2021**, *39* (11), 3051−3063.
(10) Nam, J.-W.; Kang, G.-Y.; Han, A.-R.; Lee, D.; Lee, Y.-S.; Seo, E.-K. Diarylheptanoids from the Seeds of Alpinia katsumadai as Heat Shock Factor 1 Inducers. *J. Nat. Prod.* **2011**, *74* (10), 2109−2115.
(11) Nam, J.-W.; Seo, E.-K. Structural Characterization and Biological Effects of Constituents of the Seeds of Alpinia katsumadai (Alpina Katsumadai Seed). *Nat. Prod. Commun.* **2012**, *7* (6), 1934578X1200700.
(12) Jiang, B.; Liang, Y.; Sun, X.; Liu, X.; Tian, W.; Ma, X. Potent inhibitory effect of Chinese dietary spices on fatty acid synthase. *Plant Foods Hum. Nutr.* **2015**, *70*, 257−262.
(13) Zhang, T.; Yamamoto, N.; Ashida, H. Chalcones suppress fatty acid-induced lipid accumulation through a LKB1/AMPK signaling pathway in HepG2 cells. *Food Funct.* **2014**, *5* (6), 1134−1141.
(14) Choi, S.-Y.; Lee, M. H.; Choi, J. H.; Kim, Y. K. 2,3,22,23-Tetrahydroxyl-2,6,10,15,19,23-hexamethyl-6,10,14,18-tetracosatetraene, an Acyclic Triterpenoid Isolated from the Seeds of Alpinia katsumadai, Inhibits Acyl-CoA : Cholesterol Acyltransferase Activity. *Biol. Pharm. Bull.* **2012**, *35* (11), 2092−2096.
(15) Won, H.; Son, M.-G.; Pel, P.; Nhoek, P.; An, C.-Y.; Kim, Y.-M.; Chae, H.-S.; Chin, Y.-W. Chemical constituents from Morus alba with proprotein convertase subtilisin/kexin type 9 expression and secretion inhibitory activity. *Org. Biomol. Chem.* **2023**, *21* (13), 2801−2808.
(16) Pel, P.; Chae, H.-S.; Nhoek, P.; Kim, Y.-M.; An, C.-Y.; Yoo, H.; Kang, M.; Kim, H. W.; Choi, Y. H.; Chin, Y.-W. Chemical Constituents from the Roots and Rhizomes of Sophora tonkinensis and Their Effects on Proprotein Convertase Substilisin/Kexin Type 9 Expression. *ACS Omega* **2022**, *7* (24), 20952−20958.
(17) Jang, H.-J.; Lee, S.-J.; Lee, S.; Jung, K.; Lee, S. W.; Rho, M.-C. Acyclic Triterpenoids from Alpinia katsumadai Inhibit IL-6-Induced STAT3 Activation. *Molecules* **2017**, *22* (10), 1611.
(18) Lim, H. J.; Bak, S. G.; Lim, H. J.; Lee, S. W.; Lee, S.; Ku, S.-K.; Park, S.-I.; Lee, S.-J.; Rho, M.-C. Acyclic Triterpenoid Isolated from Alpinia katsumadai Alleviates Formalin-Induced Chronic Mouse Paw Inflammation by Inhibiting the Phosphorylation of ERK and NF-κB. *Molecules* **2020**, *25* (15), 3345.
(19) Hwang, K. S.; Kim, Y. K.; Kim, Y. T.; Lee, J.; Park, K. W. A tetracosatetraene as larvicidal compound isolated from Alpinia katsumadai. *Ind. Crops Prod.* **2017**, *109*, 786−789.
(20) Wang, J.; Guo, Y.; Yin, X.; Wang, X.; Qi, X.; Xue, Z. Diverse triterpene skeletons are derived from the expansion and divergent evolution of 2, 3-oxidosqualene cyclases in plants. *Crit. Rev. Biochem. Mol. Biol.* **2022**, *57* (2), 113−132.
(21) Ghosh, S. Biosynthesis of Structurally Diverse Triterpenes in Plants: the Role of Oxidosqualene Cyclases. *Proc. Indian Natl. Sci. Acad.* **2016**, *82*, 1189−1210.
(22) Kellenbach, E. R.; Dukor, R. K.; Nafie, L. A. Absolute configuration determination of chiral molecules without crystallisation by vibrational circular dichroism (VCD). *Spectrosc. Eur.* **2007**, *19* (4), 15−17. https://www.spectroscopyeurope.com/article/absolute-configuration-determination-chiral-molecules-without-crystallisation-vibrational (accessed 2023−06−26)
(23) Freedman, T. B.; Cao, X.; Dukor, R. K.; Nafie, L. A. Absolute configuration determination of chiral molecules in the solution state using vibrational circular dichroism. *Chirality* **2003**, *15* (9), 743−758.
(24) Felippe, L. G.; Batista Jr, J. M.; Baldoqui, D. C.; Nascimento, I. R.; Kato, M. J.; He, Y.; Nafie, L. A.; Furlan, M. VCD to determine absolute configuration of natural product molecules: secolignans from Peperomia blanda. *Org. Biomol. Chem.* **2012**, *10* (21), 4208−4214.
(25) Mukai, Y.; Okamoto, R.; Takeuchi, S. Quantum fourier-transform infrared spectroscopy in the fingerprint region. *Opt. Express* **2022**, *30* (13), 22624−22636.
(26) Pavia, D. L.; Lampman, G. M.; Kriz, G. S. Introduction to Spectroscopy. *Infrared Spectroscopy*, 3rd ed.; Thomson Learning, 2001; pp 26−27.
(27) Kuroyanagi, M.; Noro, T.; Fukushima, S.; Aiyama, R.; Ikuta, A.; Itokawa, H.; Morita, M. Studies on the Constituents of the Seeds of Alpinia katsumadai Hayata. *Chem. Pharm. Bull.* **1983**, *31* (5), 1544−1550.
(28) Quan, Z.; Hou, A.; Goldfuss, B.; Dickschat, J. S. Mechanism of the Bifunctional Multiple Product Sesterterpene Synthase AcAS from Aspergillus calidoustus. *Angew. Chem., Int. Ed.* **2022**, *61* (13), No. e202117273.
(29) Fujioka, H.; Ohba, Y.; Hirose, H.; Murai, K.; Kita, Y. Mild and Efficient Removal of Hydroxyethyl Unit from 2-Hydroxyethyl Ether Derivatives Leading to Alcohols. *Org. Lett.* **2005**, *7* (15), 3303−3306.
(30) Prasain, J. K.; Tezuka, Y.; Li, J.-X.; Tanaka, K.; Basnet, P.; Dong, H.; Namba, T.; Kadota, S. New Diarylheptanoid from the Seeds of Alpinia blepharocalyx. *Planta Med.* **1999**, *65* (02), 196.
(31) Yu, H.; Lee, R.; Kim, H.; Lee, D. Diastereoselective Construction of trans-2-Alkyl-6-aryl-3, 6-dihydro-2H-pyrans Via Dehydrogenative Cycloetherification Promoted by DDQ. *Org. Lett.* **2021**, *23* (3), 1135−1140.
(32) You, H.; He, M.; Pan, D.; Fang, G.; Chen, Y.; Zhang, X.; Shen, X.; Zhang, N. Kavalactones isolated from *Alpinia zerumbet* (Pers.) Burtt. et Smith with protective effects against human umbilical vein endothelial cell damage induced by high glucose. *Nat. Prod. Res.* **2022**, *36* (22), 5740−5746.
(33) Kumagai, M.; Mishima, T.; Watanabe, A.; Harada, T.; Yoshida, I.; Fujita, K.; Watai, M.; Tawata, S.; Nishikawa, K.; Morimoto, Y. 5, 6-Dehydrokawain from Alpinia zerumbet promotes osteoblastic MC3T3E1 cell differentiation. *Biosci. Biotechnol. Biochem.* **2016**, *80* (7), 1425−1432.
(34) Yang, L.; Lin, J.; Zhou, B.; Liu, Y.; Zhu, B. Activity of compounds from Taxillus sutchuenensis as inhibitors of HCV NS3 serine protease. *Nat. Prod. Res.* **2017**, *31* (4), 487−491.
(35) Li, H.; Dong, B.; Park, S. W.; Lee, H.-S.; Chen, W.; Liu, J. Hepatocyte Nuclear Factor 1α Plays a Critical Role in PCSK9 Gene Transcription and Regulation by the Natural Hypocholesterolemic Compound Berberine. *J. Biol. Chem.* **2009**, *284* (42), 28885−28895.
(36) Shafabakhsh, R.; Reiner, Ž.; Hallajzadeh, J.; Mirsafaei, L.; Asemi, Z. Are anti-inflammatory agents and nutraceuticals-novel inhibitors of PCSK9? *Crit. Rev. Food Sci. Nutr.* **2021**, *61* (2), 325−336.
(37) Lipinski, C. A.; Lombardo, F.; Dominy, B. W.; Feeney, P. J. Experimental and computational approaches to estimate solubility and permeability in drug discovery and development settings. *Adv. Drug Deliv. Rev.* **1997**, *23* (1−3), 3−25.
(38) Athar Abbasi, M.; Raza, H.; Siddiqui, S. Z.; Zahra Siddiqui, S.; Adnan Ali Shah, S.; Hassan, M.; Seo, S. Y. Synthesis of novel N-(1, 3-thiazol-2-yl) benzamide clubbed oxadiazole scaffolds: Urease inhibition, Lipinski rule and molecular docking analyses. *Bioorg. Chem.* **2019**, *83*, 63−75.
(39) Bruhn, T.; Schaumlöffel, A.; Hemberger, Y.; Bringmann, G. SpecDis: Quantifying the comparison of calculated and experimental electronic circular dichroism spectra. *Chirality* **2013**, *25* (4), 243−249.
(40) Bruhn, T.; Schaumloffel, A.; Hemberger, Y.; Pescitelli, G. *SpecDis*. Version 1.70.1; JIMDO, 2017. https://specdis-software.jimdo.com.

https://doi.org/10.1021/acsomega.3c03873
ACS Omega 2023, 8, 32804−32816